EUROPEAN ORGANIZATION FOR NUCLEAR RESEARCH

CERN-PPE/96-123
22 July 1996

Construction and test of a fine-grained liquid argon preshower prototype

The RD3 Collaboration

R.A. Davis, D.M. Gingrich[1], J.L. Pinfold and N.L. Rodning
University of Alberta, Edmonton, Alberta, Canada

E. Boos and B.O. Zhautykov
HEPI, Alma-Ata, Kazakhstan

B. Aubert, A. Bazan, B. Beaugiraud, J. Boniface, J. Colas, G. Eynard, S. Jezequel, T. Leflour, O. Linossier, S. Nicoleau, F. Rival, G. Sauvage, J. Thion, D. VanDenPlas, I. Wingerter–Seez, R. Zitoun and Y.P. Zolnierowski
LAPP, Annecy, France

M. Chmeissani, E. Fernandez, Ll. Garrido, M. Martinez and C. Padilla
Univ. Autònoma Barcelona, Bellaterra, Spain

H.A. Gordon, V. Radeka, D. Rahm and D. Stephani
Brookhaven National Laboratory, Upton, USA

L. Baisin, J.C. Berset, J.L. Chevalley, F. Gianotti[2], O. Gildemeister, C.P. Marin, M. Nessi, L. Poggioli, W. Richter and V. Vuillemin
CERN, Geneva, Switzerland

J.M. Baze, L. Gosset, P. Lavocat, J.P. Lottin, B. Mansoulié, J.P. Meyer, J.F. Renardy, J. Schwindling and J. Teiger
CEA, DSM/DAPNIA/SPP, CE Saclay, Gif–sur–Yvette, France

J. Collot, P. de Saintignon, D. Dzahini, J.Y. Hostachy[3], A. Hoummada[4], G. Laborie and G. Mahout
ISN - IN2P3 / Université Joseph Fourier, Grenoble, France

L. Hervas
Univ. Autònoma Madrid, Spain

A. Chekhtman, M.C. Cousinou, P. Dargent, B. Dinkespiller, F. Etienne, P. Fassnacht, D. Fouchez, L. Martin, A. Miotto, E. Monnier, E. Nagy, C. Olivetto and S. Tisserant
CPP Marseille, France

G. Battistoni, D.V. Camin, D. Cavalli, G. Costa, L. Cozzi, N. Fedyakin, A. Ferrari, L. Mandelli, M. Mazzanti, L. Perini, S. Resconi and P. Sala
Dipartimento di Fisica dell'Università e Sezione INFN, Milano, Italy

[1] Also at TRIUMF, Vancouver, B.C., Canada.
[2] Also University of Milano, Italy.
[3] Corresponding author, e-mail: hostachy@isnhp2.in2p3.fr
[4] Guest professor of Université Joseph Fourier in 1993-94. Permanent address: Faculté des Sciences Aïn Chock B.P. 5366 Maârif Casablanca, Morocco.

G. Beaudoin, P. Depommier, E. León-Florián, C. Leroy and P. Roy
University of Montreal, Montreal, Canada

E. Augé, R. Chase, J.C. Chollet, C. de La Taille, L. Fayard, D. Fournier, A. Hrisoho, B. Merkel, J.M. Noppe, G. Parrour, P. Pétroff, A. Schaffer, N. Seguin–Moreau, L. Serin, V. Tisserand and I. Vichou
LAL, Orsay, France

B. Canton, J. David, J.F. Genat, D. Imbault, O. Le Dortz, A. Savoy-Navarro and P. Schwemling
LPNHE, Universités de Paris VI et VII, Paris, France

L.O. Eek, B. Lund-Jensen and J. Söderqvist
Royal Institute of Technology, Stockholm, Sweden

M. Lefebvre and S. Robertson
University of Victoria, British Columbia, Canada

Abstract

A separate liquid argon preshower detector consisting of two layers featuring a fine granularity of $2.5\ 10^{-3}$ was studied by the RD3 collaboration. A prototype covering approximately 0.8 in pseudo-rapidity and 9 degrees in azimuth was built and tested at CERN in July 94. CMOS and GaAs VLSI preamplifiers were designed and tested for this occasion. The combined response of this detector and an accordion electromagnetic calorimeter prototype to muons, electrons and photons is presented. For minimum ionizing tracks a signal-to-noise ratio of 4.5 per preshower layer was measured. Above 150 GeV the space resolution for electrons is better than 250 μm in both directions. The precision on the electromagnetic shower direction, determined together with the calorimeter, is better than 4 mrad above 50 GeV. It is concluded that the preshower detector would adequately fulfil its role for future operation at CERN Large Hadron Collider.

Submitted to *Nucl. Instr. and Meth.*

1 Introduction

The idea of equipping the accordion liquid argon (LAr) electromagnetic calorimeter, designed for the future large hadron collider (LHC) at CERN, with a fine-grained preshower detector is dictated by several requirements. A device is needed to independently measure the energy lost in the inactive material upstream of the calorimeter, thereby preserving the energy resolution for electrons and photons. By combining the position measurement of the first calorimeter compartment with that of the preshower, a precise determination of photon direction can be derived which prevents the angular term from deteriorating significantly the H$\rightarrow \gamma\gamma$ mass resolution. Furthermore, it has been shown [1] that a jet rejection factor of 10^4 is needed to reduce the huge background contribution stemming from γ-jet QCD events below the H$\rightarrow \gamma\gamma$ signal. This poses the requirement on the preshower-calorimeter system to supply a rejection factor better than 3 against isolated π^0's that dominate the background after calorimeter cuts.

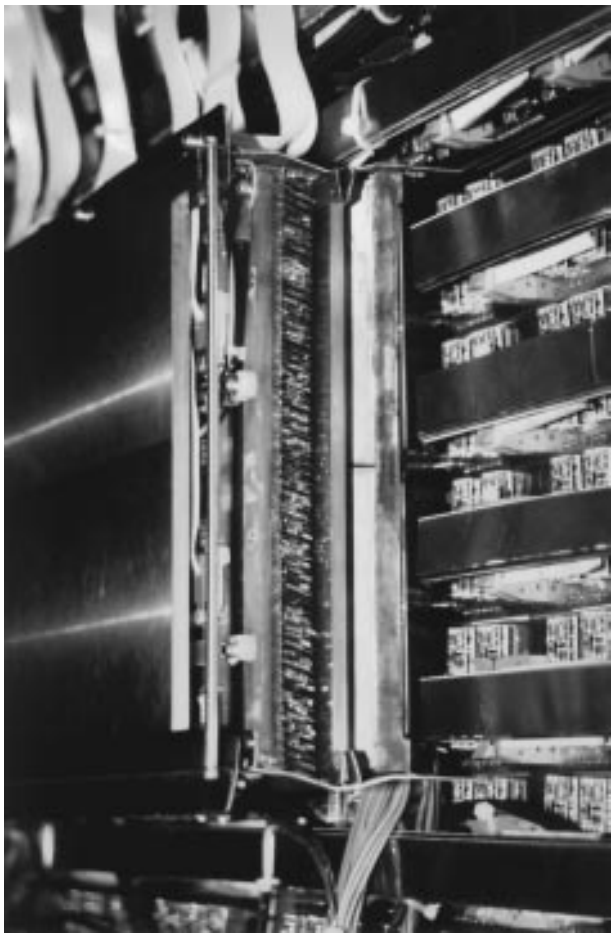

Figure 1: Photograph of the preshower detector prototype.

The potential of a fine-grained preshower was explored with a small prototype (6×6 cm^2) at CERN a few years ago [2]. The obtained performance showed the adequacy of the concept regarding the LHC requirements. Here we present a study of a modular system that constitutes a step forward in the integration of such a preshower into the ATLAS calorimetry system. For more details, refer to [3].

2 Detector geometry

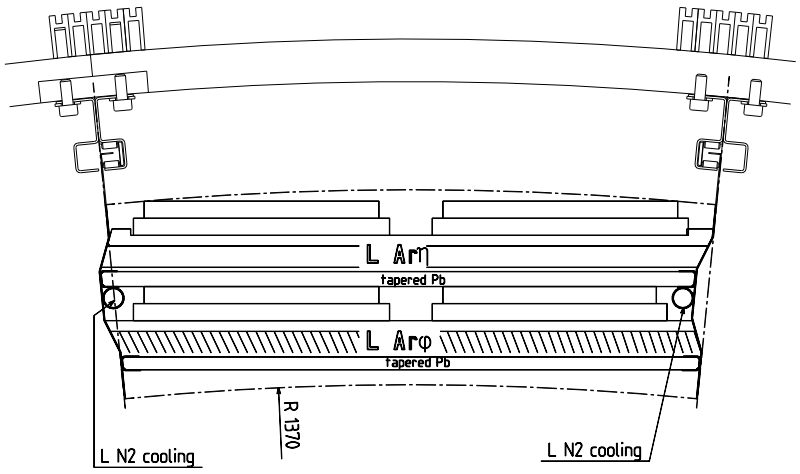

Figure 2: Transverse cut of the ATLAS preshower detector.

The preshower detector is placed in front of the accordion electromagnetic calorimeter inside the barrel cryostat. It is composed of 2 active layers of liquid argon measuring the η and the ϕ coordinates of the incident particle (see figure 2). In order to convert photons, each layer is preceded by a slab of lead. The choice of having 2 X_0 (including the upstream inactive material) in front of the first active layer and 3 X_0 in front of the second one was determined by Monte Carlo simulations [4]. The actual lead thickness is a function of the longitudinal position to keep the amount of traversed material rapidity-independent. The ideal curved structure in ϕ was abandoned in favor of a polygonal one which is easier to build. A typical structure would be 32 identical azimuthal sectors ($\Delta\phi = 11.25°$) of 3.1 m length covering half a barrel (pseudo-rapidity up to 1.5). Each azimuthal sector would be composed of 16 modules (8 per view) of 27 cm in width, supported by 2 lateral thin skirts made of stainless steel sliding on mini-rails anchored in front of the e.m. calorimeter.

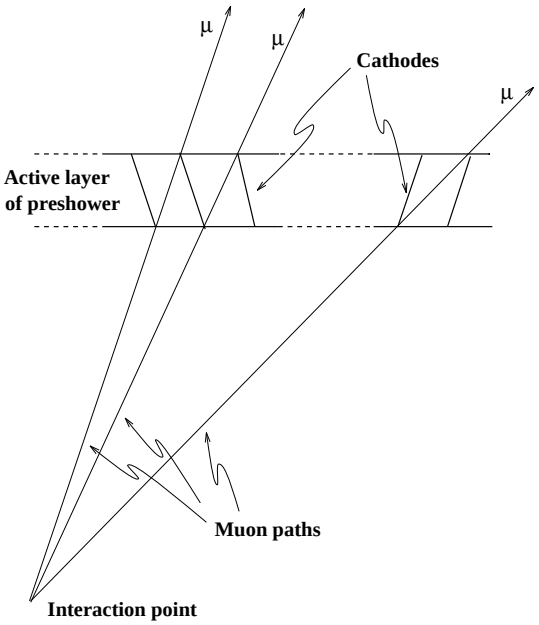

Figure 3: Principle of the electrode inclination defining an elementary cell.

A module is built up by alternating anode and cathode electrodes defining the electrical field for the charge collection in the 10 mm thick LAr gap. The electrodes of each module are slanted so that they offer a 100% geometric efficiency to muons (i.e. a muon will pass through at most two cells). This is shown in figure 3; such a design improves the space resolution. Because this ideal arrangement requires a different inclination for each cell, which is in practice difficult to achieve, we have opted for a simpler geometry. In the η layer of the preshower, the inclination of the cells is the same throughout a module, i.e. changes every 64 cells. In the ϕ layer, the cell inclination changes every eight cells. The variation in inclination in the ϕ layer is needed because of the polygonal shape as opposed to the circular one. The electric field is 1 kV/mm for the whole detector.

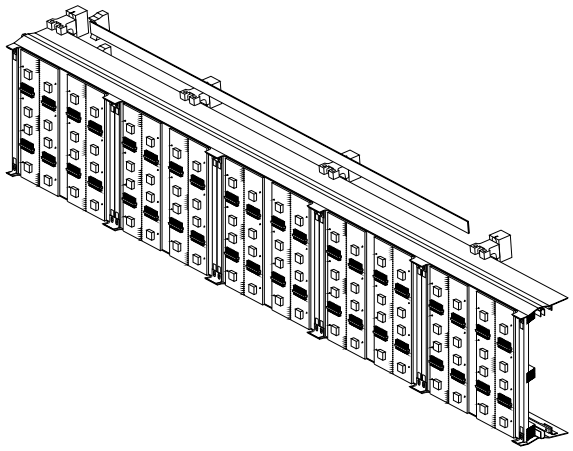

Figure 4: View of a part of the sector prototype. Only the first layer is represented. During the test, the first module was not installed. The 3 η modules were placed behind this row.

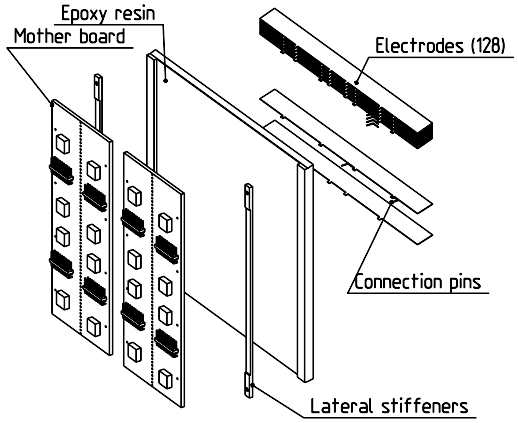

Figure 5: Exploded view of a module.

A prototype has been built by the RD3 collaboration, see figure 1. Its dimensions are slightly different from those quoted previously in order to match the existing 2 m prototype of the electromagnetic (e.m.) calorimeter [5]. It covers 9° in ϕ which corresponds to one e.m.

calorimeter module, and a pseudo-rapidity range of approximately 0.2 to 0.8, see figure 4. The granularity is $\Delta\phi \times \Delta\eta = 0.0025 \times 0.08$ and $\Delta\phi \times \Delta\eta = 0.08 \times 0.0025$ for the ϕ and η layer respectively. Seven modules were installed: 4 in the first (ϕ) layer and 3 in the second one (η). Each module reads 64 elementary intervals in the fine-grained direction and 2 in the coarse one; therefore there are 128 individual cells per module, see figure 5.

A first lead layer complements the amount of material (cryostat, beam instruments) to a constant thickness of 2 X_0 before the ϕ active layer and a second one adds one more radiation length in front of the second active layer.

3 Module production technique

A preshower module is produced by moulding a layer of epoxy on top of the electrodes stacked in a hermetic mould and precisely positioned with spacing shims. The electrodes (both cathodes and anodes) are about 19 cm long and separated by a distance of the order of 2 mm. Cathodes are made of Cu-Be and are 0.2 mm thick. Anodes are multi-layer kapton electrodes with Cu-clad HV pads on their external faces, and are 0.25 mm thick on average. Numerous tests were performed to select the epoxy system and the composite structure in order to obtain a correct cryogenic behavior of the modules. The epoxy resin finally selected (CIBA - GEIGY system MY745, HY905, DY072) is loaded with micro glass fibers (50% in weight). Its relative shrinkage coefficient from room temperature to LN_2 temperature is $\Delta L/L = 0.7$ %. Moreover, to obtain an object remaining flat when cooled down to LN_2 temperature, we had to insert glass-epoxy reinforcement bars buried in the epoxy resin. Some of them are placed along the lateral edges, the others are laid down in the x and y directions; they further reduce the shrinkage coefficient of the composite object down to a value comparable to the usual glass epoxy used in the printed circuits ($\Delta L/L = 0.36$ %). The resin after outgassing is injected with the mould placed in a vacuum-oven. A differential pressure of 0.3 bar is applied during the injection. The polymerization cycle lasts 16 h and reaches 130 °C. After unmoulding and ethanol cleaning, NOMEX honeycomb strips are slid into the cells to safely maintain the liquid argon gap. Such a module was irradiated in liquid argon with neutrons at SARA [6] up to a fluence as high as $2\ 10^{14}$ neutrons.cm^{-2}. After the irradiation, no mechanical or electrical damages were observed.

4 Electronics

Given the high channel density of such a detector, VLSI techniques have to be employed to design the front-end electronics. This work started by designing and producing octal preamplifier chips in CMOS and in GaAs monolithic processes.

4.1 CMOS preamplifiers

ICON is a current conveyer preamplifier based on a layout that was originally considered for the readout of silicon detectors [7]. To meet the particular needs of the LAr calorimetry, some improvements had to be made regarding the current gain and the noise. This study was carried out using CMOS monolithic processes of three different firms: MIETEC, ES2 and AMS; see table 1. So far the best performance with respect to the speed was measured at 77 °K on the AMS 1.2 μm version ($t_p^{5-100\%}$(260 ns triangle)=62 ns when filtered by a CR-RC^2 filter of 25 ns shaping time), with an equivalent noise current at its input of 19 nA for a detector capacitance of 20 pF and a 25 ns CR-RC^2 shaping time. Being the only ones available at that time, 512 channels of the MIETEC version, which has a lower performance in terms of speed, were used to equip 4 preshower modules in July 94.

Table 1: Measured performance of ICON preamplifiers from three different manufacturers

Type (bias voltage)	MIETEC (± 4.5 V)	ES2 (± 4 V)	AMS (± 3.5 V)
27°C peaking time (5-100%) on a Dirac	64 ns	30 ns	14 ns
77°K peaking time (5-100%) on a Dirac	40 ns	25 ns	12 ns
Noise at 20°C, (no filter) (ENC: e^-) (10 pF)	4400	4200	4000
Noise at 77°K, (no filter) (ENC: e^-)	2200+50/pF	1900	2400+30/pF
20°C (20% ICON - 80% Buffer)	35 mW	55 mW	20 mW
77°K power dissipation (20% ICON - 80% Buffer)	51 mW	70 mW	23 mW

4.2 GaAs preamplifiers

The second device under study is a monolithic charge-sensitive preamplifier made with a GaAs ion-implanted MESFET process [8]. The chip contains dominant pole preamplifiers with a gain-bandwidth product of about 1 GHz. The preamplifier input capacitance is 12 pF. The series noise at liquid argon temperature, 87°K, is 0.84 nV/$\sqrt{Hz}$ on average (0.54 nV/$\sqrt{Hz}$ for the best chips), and the corner frequency of the 1/f noise does not reach 1 MHz. Its power dissipation is 7.5 mW. With CR^2-RC^2 bipolar shaping an equivalent noise current of 6.9 nA on average was obtained at 87°K for a detector capacitance of 20 pF and a peaking time of 28 ns on a Dirac pulse. 384 channels of that type were mounted on 3 preshower modules for the July 94 test beam period.

4.3 Mother boards

Fourteen mother boards (MB's), made of Cobrisol which is a material similar to G10, were needed to read the whole RD3 preshower prototype in the test beam. They were 8 cm wide and their length, which varied according to the module, were of the order of 20 cm. Each MB had 6 layers and its overall thickness was 1.2 mm which was a compromise to make the MB as thin as possible and to keep some rigidity to tolerate the mechanical stress during mounting and dismounting operations. The MB was directly mounted on the preshower detector and the contacts were established through 64 holtite female connectors. The MB contraction at LAr temperature was similar to the value given by a preshower module, (see section 3). The soldered components were SMD type in order to keep the total thickness of the PCB, its components and the pile-up of 10 read-out cables, less than 20 mm. We used Phillips diodes BAV99 to protect the inputs of the preamplifiers. NPO capacitors and resistors with temperature coefficient 100 ppm/°C were used to cope with the low temperature of LAr.

A test pulse system was implemented to be used as a diagnostic and calibration means. For this we made a trace 3 mm wide on the mother board internal layer, and on the component layer we printed a solid rectangle of 3×4 mm^2 size at each input trace of the preamplifier above the position of the 3 mm internal trace. This design creates a 4 pF capacitance, which is big enough to inject a small current test pulse with approximately 260 ns fall time. This test pulse system allows us to calibrate the preshower with an accuracy of about 10%.

4.4 Read-out

Signals from the preshower were brought out of the cryostat via Fileca[5] 16 channel cables of 50 Ω characteristic impedance. The outputs from the GaAs preamplifiers were filtered by $(CR)^2$-$(RC)^2$ shapers of 25 ns time constant. The shaped signals were sampled at the peak with Track&Hold units and digitized by 12-bit ADC's. The signals from the CMOS preamplifiers were integrated in 40 ns gated integrators and their outputs were read out by 12-bit ADC's.

5 Performance in a test beam

For the beam tests, the preshower was installed in front of the accordion electromagnetic calorimeter prototype [5] and was cooled down inside the same cryostat. The calorimeter was segmented into three radial compartments of 9 X_0, 9 X_0 and 7 X_0 respectively. The granularity of the e.m. calorimeter was $\Delta\phi \times \Delta\eta = 0.02 \times 0.018$ for the first two radial compartments and $\Delta\phi \times \Delta\eta = 0.02 \times 0.036$ for the third one.

The test was performed on the H8 beam line of the CERN SPS with electrons and photons. Muon data were also collected by exploiting the large μ contamination in the electron beam around 150 GeV/c.

The beam line was equipped with four fast scintillation counters, used in the trigger, and three drift chambers which allowed to reconstruct the particle impact point at the front face of the preshower.

A simulation of the setup has been performed, using GEANT. More details about the simulation can be found in [9], where most of our results are reported and compared to the experimental ones obtained during the July 94 test run.

5.1 Shower profiles

The average profiles of photon and electron showers in each layer of the preshower are shown in figure 6. For both particle types the shower is seen to be slightly broader in the η layer than in the ϕ layer due to the extra X_0 of lead before the η sampling. Photons have slightly thinner profiles than electrons due to later shower production, which is confirmed in the simulation. The percentages of the total energy found within a 3-cell cluster for various photon energies are shown in table 2. In both cases it can be seen that the variations in the shower profile widths with energy and position are small and therefore a universal cluster of 3-cell size can be used to determine the position of the incident particle. For energy measurements a larger cluster will be more appropriate.

Table 2: Simulation of the percentage of the total energy deposited by a photon within a 3-cell preshower cluster, for a few different photon energies and pseudo-rapidities.

E_γ (GeV)	η	% of energy in preshower cluster	
		ϕ layer	η layer
54.5	0.26	92.0	90.0
78.3	0.26	91.9	91.0
104.7	0.26	91.8	90.6
33.4	0.37	93.7	91.6
65.9	0.37	93.4	91.0
106.3	0.37	93.5	90.7

[5] Manufactured by FILECA, Sainte Geneviève, France

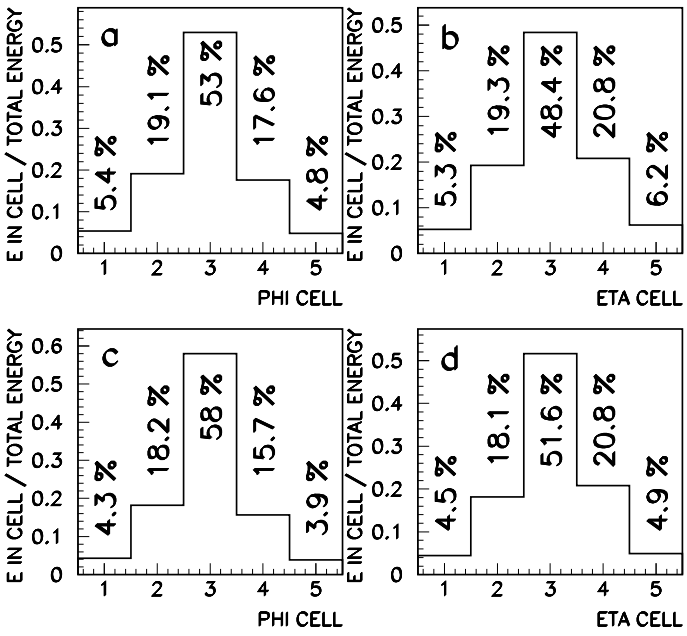

Figure 6: Shower profiles: a and b for a 200 GeV electron at $\eta \simeq 0.3$ in the preshower ϕ and η layers respectively; c and d for a 105 GeV photon at $\eta \simeq 0.26$ in the preshower ϕ and η layers respectively.

5.2 Off-line calibration

The off-line calibration was performed by equalizing the response of the cell triplets with 200 GeV electrons. The new gains (calculated cell by cell) are then introduced in the off-line analysis program. This operation is repeated at least once because the calculation of the position barycenter depends on the gains. Then the absolute normalization factor is deduced from the muon peak which is expected at 2.11 MeV on average for 10 mm of active LAr at $\eta = 0$. The sigma of the average response after off-line calibration was of the order of 2%.

5.3 S-shape corrections

The position of electrons and photons is determined using a barycentric calculation within a cell cluster. The resulting distribution of the beam particle position is periodic because of the discrete structure of the detector (period of one cell). In figure 7 the profile of the η impact position (expressed in cell units) using the beam chambers is plotted as a function of the position determined with the preshower. Such a variation can be corrected using a S-shape function[6]:

$$\eta_{\rm TRUE} = a_0 + a_1.round(\eta_{\rm PS}) + a_2.(round(\eta_{\rm PS}))^2 + a_3.tan^{-1}[a_4.(\eta_{\rm PS} - round(\eta_{\rm PS}))]$$

where the last term describes the pattern and the first three give the global position (practically along a straight line). The same method was applied to correct the ϕ preshower impact position.

[6] round(x) $\equiv$ closest integer to x

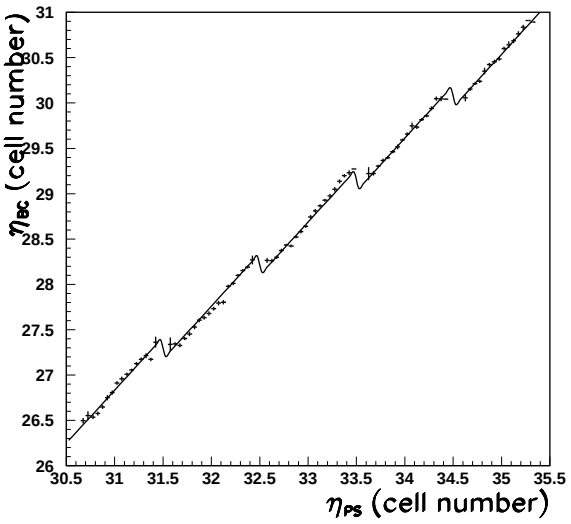

Figure 7: Profile of the impact position given by the beam chambers against the position found using the preshower. The fitted correction function is superimposed. The cell width in this preshower module is 3.2 mm.

5.4 Response to muons

For each view, the muon signal was reconstructed by adding the contributions of two adjacent cells: the most energetic one and its most energetic neighbor found in a window of 5 cells centered on the extrapolated beam impact point. This signal is plotted in figure 8. The signal/noise ratio ($\langle \text{signal} \rangle / \sigma(\text{noise})$) is about 4.5 per preshower layer with GaAs preamplifiers and 4.0 with CMOS preamplifiers. The electronic noise was measured with random trigger events by choosing the signals of two adjacent cells randomly within the beam impact profile.

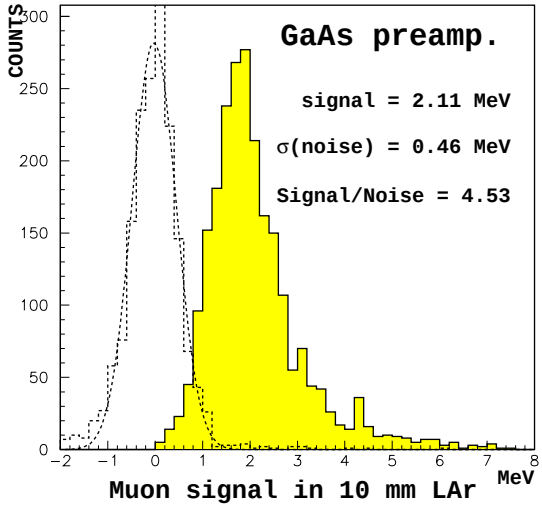

Figure 8: Muon signal in one preshower layer read out by GaAs preamplifiers.

The space resolution, after S-shape function correction and after unfolding the contribution due to the beam chambers (~250 μm in both directions at 150 GeV), is of the order of 860 μm.

5.5 Response to electrons

5.5.1 Dynamics of the electron signal

Figure 9 shows the maximum of deposited energy in one cell by electrons (in MIP) with 95% acceptance in each layer and at $\eta = 0.3$. The plotted curves are parametrized as $a_1 E^{a_2}$ where $a_1 = 7.78 \pm 0.16$ and 10.2 ± 0.15 and $a_2 = 0.385 \pm 0.005$ and 0.538 ± 0.003 for the η and ϕ layers respectively. These dynamics curves extrapolated to 2 TeV give a deposited signal of 611 ± 25 MIP in the η layer and 146 ± 9 MIP in the ϕ layer. For a signal/noise ratio of 4 per layer, the required dynamic range in η is approximately 12 bits and 2 bits less in the ϕ layer. The simulation results are close to our extrapolated values, 609 ± 22 MIP in η and 164 ± 9 MIP in ϕ.

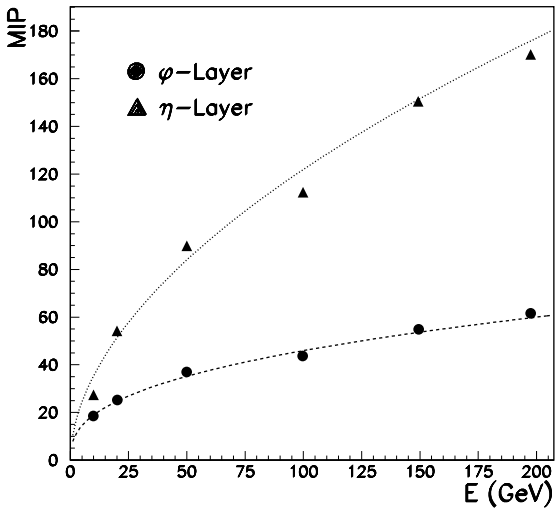

Figure 9: Maximum of deposited energy in one cell by electrons (in MIP) with 95% acceptance in each layer and at $\eta = 0.3$. (95% of the electrons fall bellow the plotted value).

5.5.2 Energy resolution

The energy deposited by 287 GeV electrons is presented in figure 10. The electron signal was collected over a calorimeter cell nonet and 100 (50/layer) cells in the preshower centered on the most energetic channel. The represented quantity is the total energy obtained as $E_{tot} = \lambda(\alpha E_{psh} + \beta E_1 + E_2 + E_3)$, where E_{psh}, E_1, E_2, E_3 refer to the signals collected in the preshower and the three calorimeter radial compartments, α and β are energy dependent weights introduced to minimize the width of the energy distribution and λ is an overall calibration coefficient. Standard position-dependent energy corrections determined at 287 GeV were applied to the calorimeter in order to correct for the shower containment in η and the modulation of the transverse LAr thickness in ϕ [5].

The energy resolution of the preshower-calorimeter system at $\eta = 0.3$ is plotted in figure 11 and parameterized as:

$$\frac{\sigma_E}{E} = \frac{(12.5 \pm 0.3)\%}{\sqrt{E(\mathrm{GeV})}} \oplus \frac{(337 \pm 20)}{E(\mathrm{MeV})} \oplus (0.45 \pm 0.06)\%$$

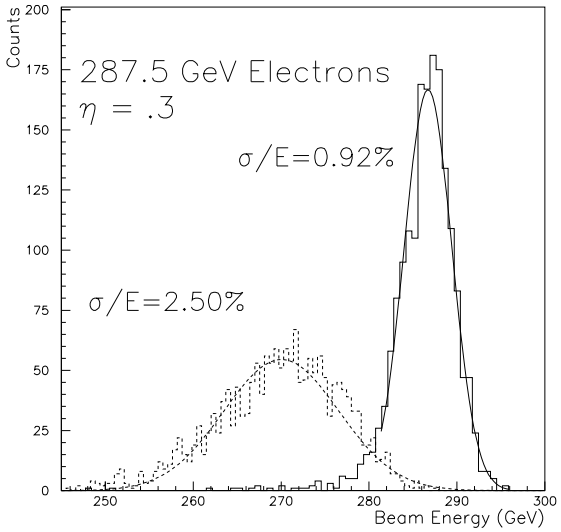

Figure 10: Energy reconstructed in the preshower-calorimeter system from 287 GeV e^- before (dashed) and after (solid) adding the preshower contribution.

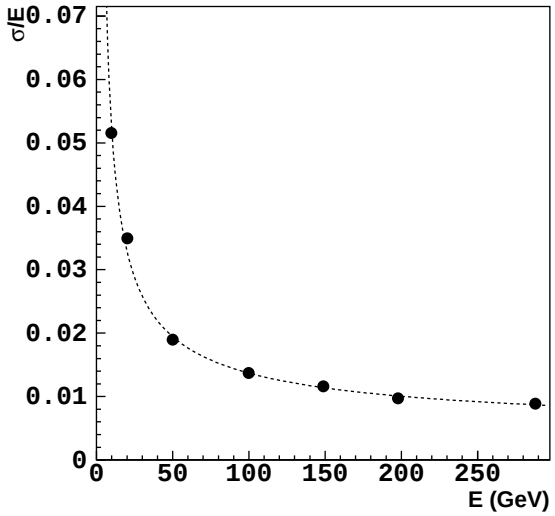

Figure 11: Energy resolution as a function of the incident electron energy measured at $\eta = 0.3$.

This can be compared to Monte-Carlo simulations shown in table 3, for which the energy resolution was parameterized as:

$$\frac{\sigma_{\mathrm{E}}}{E} = \frac{a}{\sqrt{E}} \oplus b$$

Electronic noise and pile-up effects (which would contribute a term proportional to 1/E) were not simulated. The experimental result is in good agreement with the predictions. The large value of the sampling term (12.5%) is due to the fact that the dead space between the preshower and the calorimeter was too large (~10 cm). A new simulation made at $\eta = 0.26$, with only 5 cm between the preshower and the calorimeter, led to the following energy resolution:

$$\frac{\sigma_{\mathrm{E}}}{E} = \frac{(10.5 \pm 0.2)\%}{\sqrt{E(\mathrm{GeV})}} \oplus (0.40 \pm 0.06)\%$$

Table 3: Energy resolution of the preshower-calorimeter system estimated by Monte-Carlo simulation

	η=0.1	η=0.26	η=0.37	η=0.57
a ($\frac{\%}{\sqrt{GeV}}$)	11.6 ($\pm$0.2)	11.9 ($\pm$0.2)	12.4 ($\pm$0.2)	12.7 ($\pm$0.2)
b (%)	0.18 ($\pm$0.15)	0.36 ($\pm$0.06)	0.16 ($\pm$0.1)	0 ($\pm$0.2)

The dead zone between the preshower and the calorimeter is a critical point because it corresponds to a stage of the shower where a significant fraction of the particle energy can be deposited. This distance will be reduced in the final design by making use of compact connections and cablings.

5.5.3 Linearity of the response

The linearity has been estimated by comparing the average energy of the preshower-calorimeter system, after energy correction and absolute calibration at 150 GeV, with the nominal energy of the beam, see figure 12. In this picture, the two dotted curves represent the uncertainties on the beam momentum, i.e.:

$$\frac{\Delta P}{P} = \frac{25}{P}\% \oplus 0.5\% \text{ (P in GeV)}$$

where the first term is linked to the hysteresis effect of the bending magnet and the second term includes the uncertainties due to geometry and calibration.

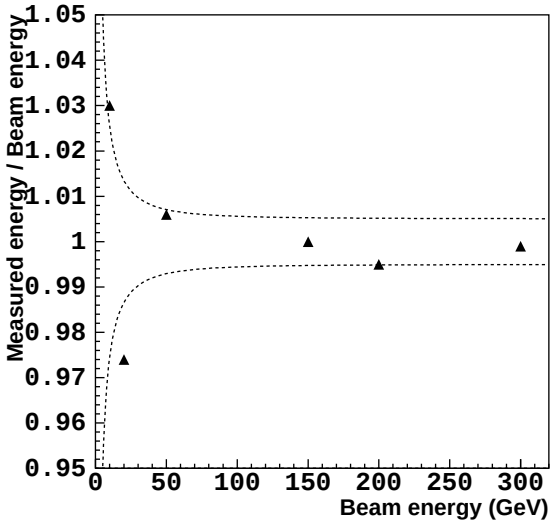

Figure 12: Linearity of the preshower-calorimeter response function of the electron energy. The two dotted curves represent the uncertainties on the beam momentum, see text.

5.5.4 Space resolution

The electromagnetic shower positions (ϕ and η) were reconstructed as the energy-weighted barycenter of the three adjacent cells consisting of the most energetic one and its two neighbors. Both positions were also provided by means of 3 beam chambers. The space resolution at $\eta = 0.3$ as a function of the incident electron energy, after S-shape correction and after unfolding the contribution due to the beam chambers ($\sigma \simeq 270\ (530)\ \mu$m at 200 (10) GeV), is given in figure 13.

The curves which are superimposed on the data points,

$$\sigma_\phi = \frac{(2.02 \pm 0.03)}{\sqrt{E(\mathrm{GeV})}} \oplus (0.19 \pm 0.004)\ \mathrm{mm}$$

$$\text{and } \sigma_\eta = \frac{(1.67 \pm 0.03)}{\sqrt{E(\mathrm{GeV})}} \oplus (0.16 \pm 0.004)\ \mathrm{mm},$$

agree very well with the predictions of Monte-Carlo simulations (see table 4). The space resolution is slightly better in the η layer where the signal is larger owing to the additional lead placed at the front. Above 200 GeV, the position resolution is better than 230 μm in both coordinates.

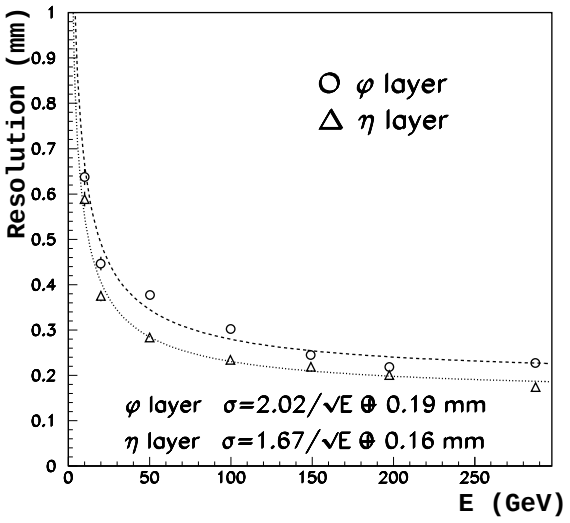

Figure 13: Space resolution of the preshower after S-shape correction and unfolding of the beam chamber contribution.

Table 4: Simulated space resolution for electrons at different η-values

η	ϕ layer (mm)	η layer (mm)
0.1	$\frac{1.80(\pm 0.05)}{\sqrt{E}} \oplus 0.22(\pm 0.01)$	$\frac{1.55(\pm 0.06)}{\sqrt{E}} \oplus 0.19(\pm 0.01)$
0.26	$\frac{1.79(\pm 0.07)}{\sqrt{E}} \oplus 0.25(\pm 0.01)$	$\frac{1.62(\pm 0.06)}{\sqrt{E}} \oplus 0.17(\pm 0.01)$
0.37	$\frac{2.09(\pm 0.1)}{\sqrt{E}} \oplus 0.22(\pm 0.01)$	$\frac{1.59(\pm 0.08)}{\sqrt{E}} \oplus 0.17(\pm 0.01)$
0.57	$\frac{1.91(\pm 0.02)}{\sqrt{E}} \oplus 0.24(\pm 0.01)$	$\frac{1.63(\pm 0.07)}{\sqrt{E}} \oplus 0.21(\pm 0.01)$

5.5.5 Angular resolution

The preshower and calorimeter information can be combined to determine the direction of the incoming electron through the measurements of the shower position at two different depths; in our case the preshower and the first compartment of the calorimeter were used. The angle of

the incident particle is then given, in the η and ϕ directions, by

$$\theta_{\rm i} = \arctan(\frac{d_{\rm i,calo} - d_{\rm i,ps}}{D_{\rm i}}),$$

where the numerator is the difference between the shower $d_{\rm i}$ positions reconstructed in the two detectors and the denominator $D_{\rm i}$ is the average lever arm estimated with a Monte-Carlo simulation program, see table 5. In fact, the calculation of the angular resolution in η is slightly more complicated because the electron beam is not perpendicular to the η layer. This involves a factor $\sin(\theta)$ in the definition of $\rm d_i$ when using the longitudinal position given by the η layer. For the same event, the angles $\theta_{\rm i}$ are then compared to the angles measured using the first and the last beam chambers, located upstream of the cryostat, and separated by 11.124 m. Figure 14 shows the angular resolution at $\eta = 0.3$, in both directions, as a function of the incident electron energy. The angular resolution can be fitted as

$$\sigma_\phi = \frac{(27.6 \pm 0.2)}{\sqrt{E(\rm GeV)}} \oplus (1.0 \pm 0.05)\ \rm mrad$$

$$\text{and } \sigma_\eta = \frac{(22.3 \pm 0.2)}{\sqrt{E(\rm GeV)}} \oplus (0 \pm 0.2)\ \rm mrad.$$

The very good angular resolution is partly due to the lever arms which are about 25% longer than in the final design with a closer distance to the calorimeter. The Monte Carlo predictions given in table 6 are in fair agreement with the measured results.

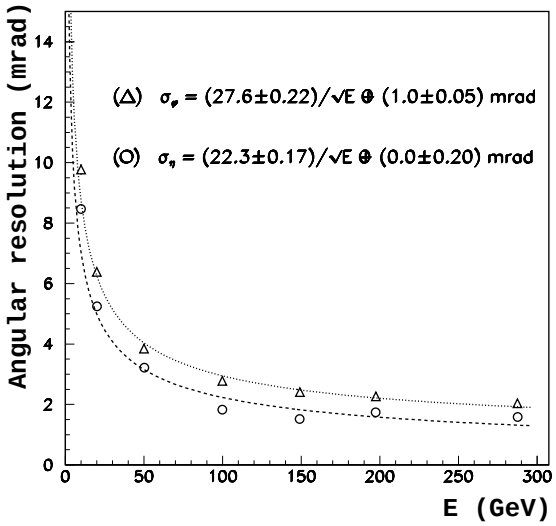

Figure 14: Angular resolution in both directions of the combined preshower-calorimeter system at $\eta = 0.3$ as a function of the electron energy.

The test beam divergence in both ϕ and η directions for various electron energies were small: 0.2 and 0.1 mrad at 50 GeV in ϕ and η respectively. The beam divergence is at least one order of magnitude smaller than the angular resolution; this will allow us to neglect it when considering the photon data.

Table 5: Simulated lever arms in cm for various electron energies and η-values.

pseudo-rapidity	0.26		0.37		0.57	
E(GeV)	d_ϕ	d_η	d_ϕ	d_η	d_ϕ	d_η
10	21.2	19.3			20.7	21.2
20	21.7	19.8	21.5	20.3	21.2	21.7
50	22.3	20.4			21.9	22.5
100	22.9	21.0			22.3	23.0
200	23.5	21.6	22.2	23.3	22.9	23.7
300	23.9	22.0	23.7	22.6		

Table 6: Simulated angular resolution for electrons at different η-values.

η	ϕ layer (mrad)	η layer (mrad)
0.37	$\frac{2\ .5\ (\pm 1.4)}{\sqrt{E}} \oplus 1.9(\pm 0.1)$	$\frac{25.3\ (\pm 0.5)}{\sqrt{E}} \oplus 1.(\pm 0.1)$
0.57	$\frac{28.4\ (\pm 0.2)}{\sqrt{E}} \oplus 1.2(\pm 0.3)$	$\frac{26.6\ (\pm 0.4)}{\sqrt{E}} \oplus 0(\pm 0.2)$

5.5.6 Response to photons

The experimental setup used to measure the response of the prototype to photons is shown in figure 15. The photon beam is produced by placing a slab of aluminum in the electron beam. Photons and electrons are separated with a magnet which deflects the electrons in the ϕ direction to an area of the electromagnetic calorimeter not covered by the preshower. The electron beam goes through a scintillator (S3) and two multiwire beam chambers, one before the Al radiator (BC1) and one after the magnet (BC2).

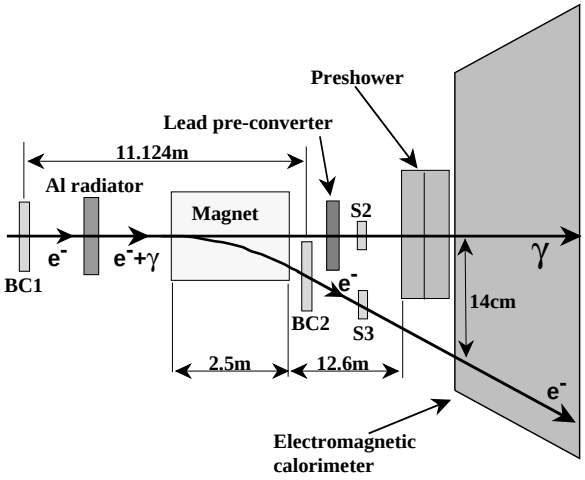

Figure 15: The photon beam setup.

It is known that a significant number of electrons will produce more than one photon in the Al radiator. In order to identify these multiple photon events, a preconverter (a $1X_0$ thick slab of lead) followed by a scintillator (S2) was placed in the photon beam. In a simulation of the experimental setup, for a 200 GeV electron beam there was a 40% multiple photon contamination without the lead and only 22% when using the preconverter, i.e. by requiring no signal in S2. The energy of the photon beam was varied between 30 and 120 GeV either by changing the

electron beam energy (150 GeV or 200 GeV) or by varying the strength of the magnetic field while keeping the position of S3 fixed.

Since there is no way of knowing the photon impact position independently of that given by the preshower detector, the photon spatial resolution cannot be measured.

The angular resolution can be measured because its calculation only involves the use of particle impacts in the preshower and the accordion calorimeter. The calculation of the photon beam divergence is however not possible. Therefore it was assumed that it is similar to that of the electron beam (i.e. $\sim$ 0.2 (0.1) mrad in ϕ (η) respectively), i.e. small compared to the Monte Carlo prediction of the angular resolution. This assumption is reasonable since, during the creation of a photon by Bremsstrahlung in which the energy of the electron in the initial and final states is large, the photon and the degraded electron are emitted within a rms angle of the order of $\theta = \frac{m_e c^2}{E}$ rad where E is the initial electron energy.

The S-shape corrections, as described in section 5.3, were performed, assuming the same behavior for photons and electrons of similar pseudo-rapidity. The angular resolution is calculated in exactly the same way as for the electron data. The photon lever arms used are shown in table 7.

Table 7: Simulated lever arms in cm for photons of various energies and pseudo-rapidities.

pseudo-rapidity	0.26		0.57	
E (GeV)	ϕ layer	η layer	ϕ layer	η layer
10	21.5	19.6	21.0	21.5
20	22.0	20.1	21.6	22.1
50	22.7	20.8	22.1	22.7
100	23.1	21.2	22.7	23.4
200	23.8	21.9		

The variation of the angular resolution with photon energy is shown in figure 16. Only three different photon beam energies were available for each of the two values of pseudo-rapidity and therefore the points for both $\eta = 0.29$ and $\eta = 0.37$ have been used to fit the two curves. One obtains:

$$\sigma_\phi = \frac{(16.2 \pm 0.3)}{\sqrt{E\ (\mathrm{GeV})}} \oplus (1.0 \pm 0.1)\ \mathrm{mrad}$$

$$\sigma_\eta = \frac{(19.2 \pm 0.5)}{\sqrt{E\ (\mathrm{GeV})}} \oplus (1.7 \pm 0.1)\ \mathrm{mrad}.$$

These values are slightly better than those derived from the simulation, see table 8. This was also observed for electrons. A suggested explanation is that in the simulation, the particle beam covered three accordion calorimeter cells whereas in the actual tests only one cell was covered.

Table 8: Simulated angular resolution for photons at different η-values.

η	ϕ layer (mrad)	η layer (mrad)
0.26	$\frac{20.9\ (\pm 0.6)}{\sqrt{E}} \oplus 1.3\ (\pm 0.1)$	$\frac{26.9\ (\pm 1.0)}{\sqrt{E}} \oplus 1.5\ (\pm 0.1)$
0.57	$\frac{21.8\ (\pm 0.8)}{\sqrt{E}} \oplus 0.84\ (\pm 0.3)$	$\frac{27.4\ (\pm 1.4)}{\sqrt{E}} \oplus 1.3\ (\pm 0.4)$

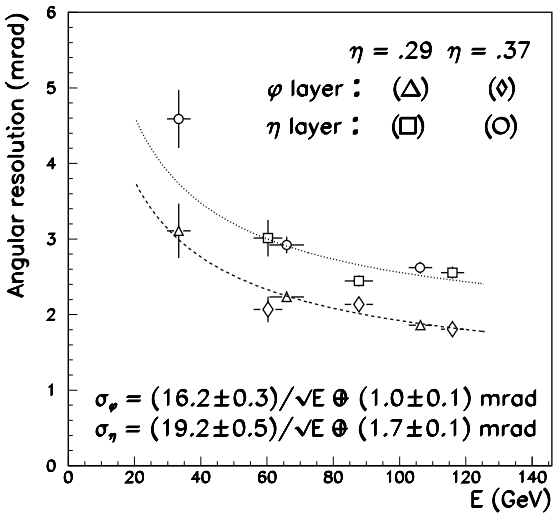

Figure 16: Angular resolution in both directions of the combined preshower-calorimeter system as a function of the photon energy. The dotted (dashed) line fits the ϕ (η) active layer results respectively.

6 Conclusions

The moulding process developed over the last three years to produce preshower modules is technologically a good candidate for larger scale construction. The performance of the prototype measured in electron, photon and muon test beams shows that this concept meets the LHC requirements especially with respect to the space and angular resolution. Although GaAs cold analog electronics seem more promising for this application, CMOS preamplifiers may constitute a good alternative solution if their resistance to ionizing radiation at LAr temperature can be achieved. The difficulty of the integration of this device in a detector such as ATLAS comes from the large number of electronic channels (115,000 for $|\eta| \leq 1.4$) to bring out of the cryostat. Analog optical links [10] that allow the reduction of the overall diameter of the cryostat feedthroughs may be envisaged. During a beam test in September 94, 32 channels of such links were successfully used for the read-out of a preshower module.

Acknowlegments

The authors wish to thank the technical staff of the participating laboratories for their skillful contribution to the construction of this prototype.

References

[1] L. Fayard and G. Unal, search for Higgs decay into photons with ATLAS, ATLAS internal note, physics-NO-001, December 91.
D. Froidevaux et al., comparison of the ATLAS and CMS discovery potential for the H$\rightarrow \gamma\gamma$ channel at the LHC, ATLAS internal note, physics-NO-064, February 95.

[2] B. Aubert et al. (RD3 Collaboration), Performance of a liquid argon preshower detector integrated with an accordion calorimeter, Nucl. Inst. and Meth. A 330 (1993) 405.

[3] RD3 Collaboration, CERN/DRDC/92-40 (1992).

[4] G. Unal, Preshower performance for gamma identification, ATLAS Internal Note CAL-NO-009, July 1992.

[5] D.M. Gingrich et al. (RD3 Collaboration), Performance of a large scale prototype of the ATLAS accordion electromagnetic calorimeter, Nucl. Instr. and Meth. A 364 (1995) 290.

[6] J. Collot et al., A neutron irradiation facility featuring cryogenic temperatures and dedicated to Large Hadron Collider detector design, Nucl. Inst. and Meth. A350 (1994) 525.

[7] D. Dzahini et al., A CMOS current preamplifier and shaper with 50 Ω line driver for a liquid argon preshower, IEEE Trans. on Nucl. Sci., Vol. 42, No 4 (1995) 767.

[8] D.V. Camin, N. Fedyakin and G. Pessina, Monolithic GaAs readout for a LAr preshower detector, proceedings of the fourth international conference on calorimetry in high energy physics, La Biodola, September 1993.
D.V. Camin, G. Pessina and E. Previtali, Front-end in GaAs, Nucl. Inst. and Meth. A315 (1992) 385.

[9] G. Mahout, Thèse de l'Université Joseph Fourier de Grenoble, ISN 95.09, 1995.

[10] S. Tisserant (on behalf of the RD3 collaboration), Analog optical link in liquid argon, proceedings of the fifth international conference on calorimetry in high energy physics, BNL, September 1994, eds. H.A. Gordon and D. Rueger (World Scientific Publishing, Singapore) p 449.
B. Dinkespiler et al., Analog optical links for the liquid argon calorimeters, proceedings of the first workshop on electronics for LHC experiments, Lisbon, CERN/LHCC/95-56 Oct 95.
L.O. Eek (on behalf of the Atlas/Larg collaboration), A fine-grained liquid argon preshower detector and an analog optical link for its read-out, proceedings of the international europhysics conference on high energy physics, Brussels, July 1995.